Low Noise Near-Concentric Optical Cavity Design

Florentin Adam,[1] Wen Xin Chiew,[1] Adrian Nugraha Utama,[1] and Christian Kurtsiefer[1,2]
[1)]*Center for Quantum Technologies, 3 Science Drive 2, Singapore 117543*
[2)]*Department of Physics, National University of Singapore, 2 Science Drive 3, Singapore 117542*

(*Electronic mail: christian.kurtsiefer@gmail.com)

(Dated: 8 December 2023)

Near-concentric cavities are excellent tools for enhancing atom–light interaction as they combine a small mode volume with a large optical access for atom manipulation. However, they are sensitive to longitudinal and transverse misalignment. To address this sensitivity, we present a compact near-concentric optical cavity system with a residual cavity length variation $\delta L_{C,rms} = 0.36(9)$ Å. A key part of this system is a cage-like tensegrity mirror support structure that allows to correct for longitudinal and transverse misalignment. The system is stable enough to allow the use of mirrors with higher cavity finesse to enhance the atom–light coupling strength in cavity-QED applications.

INTRODUCTION

Establishing strong atom–light interaction is essential for the implementation of quantum networks in atomic systems[1,2]. However, interfacing with atoms can be challenging due to their small cross-section. Commonly used approaches to enhance atom–light interaction involve highly focusing lenses[3] or optical resonators[4]. For the latter, cavity quantum electrodynamics (CQED) has been extensively researched with optical resonators in various configurations[5], and demonstrated with single atoms since the 1980's [6,7]. To attain a strong atom–light coupling strength g, typically short cavities with a small mode volume and high reflectivity, low loss mirrors are used. This leads to atom–light interactions using cavity mirror spacings ranging from micrometres[8,9] to millimetres[10] with high quality factor Q. Most of the cavities for CQED involve a near-planar geometry, with a mirror separation much smaller than their radius of curvature. This allows for stable mechanical designs, but requires a short distance between the mirror surfaces.

Optical cavities in the near-concentric (NC) regime, where the length of the cavity is close to the sum of the spherical mirrors' radii of curvature, have most of the cavity modes strongly focused at the center, leading to a small effective mode volume[11] and thus a strong atom–light coupling strength g while providing easy optical access through the relatively large mirror separation.

However, NC cavities are challenging to work with compared to planar micro-cavities, as transverse displacement of the mirrors affects the cavity resonance. As the optical cavity resonance needs to have a well-defined relation to fixed atomic resonances in CQED applications, the mechanical cavity stability is critical. In NC cavities, there is the additional requirement for transverse adjustability and stability, leading to the need for control of three degrees of freedom for relative mirror positions.

Here, we present a NC configuration of an optical resonator exhibiting low susceptibility to external mechanical noise and thus stability, while maintaining adjustability in all necessary degrees of freedom. The design significantly lowers the mechanical noise compared to our previous implementation[12], while allowing us to reach the last stable point before the concentric point, and hence a stronger atom–light coupling.

CAVITY DESIGN

To facilitate atom–cavity interaction at a specific transition, in our case the D_2 line of ^{87}Rb at $\lambda = 780\,$nm with an atomic half-linewidth $\gamma = 2\pi \times 3.03\,$MHz, the cavity resonance frequency ω_C has to match with the atomic resonance frequency. To place neutral atoms at the cavity center, we use a magneto-optical trap[13] and a dipole trap[14] in an ultra-high-vacuum (UHV) environment. To retain optical access to the system, and minimize the size of magnetic coils, a small glass cuvette with inside dimensions of $25 \times 25 \times 150\,$mm is used. The NC cavity system has to fit inside this relatively small cuvette.

Stability requirement

To quantify the impact of the shift in cavity resonance and the cavity performance, we introduce a "noise limit factor" ξ which normalizes the frequency fluctuation $\delta\omega_C$ due to mechanical noise to the cavity linewidth 2κ. This factor is equivalent to the ratio of mechanical noise (standard deviation δL_C of the cavity length) to the resonant wavelength, multiplied by the cavity finesse F:

$$\xi = \frac{\delta\omega_C}{2\kappa} = \frac{\delta L_C}{\lambda/2} F. \tag{1}$$

A noise limit factor $\xi = 1$ indicates that the cavity resonance fluctuation is equal to its linewidth. Here, we aim for a target of $\xi = 0.15$, which means that the mechanical noise along the cavity axis contributes to the cavity linewidth by at most 15%.

Both transverse and longitudinal misalignments will affect the reflection and/or transmission of the NC cavity. Close to the concentric point, transverse positioning noise will dominate the deviation of the cavity resonance from the atomic transition. For convenience, however, we map all mechanical effects on the cavity resonance to effective fluctuation of the cavity length δL_C.

Mirror characteristics

The cavity mirrors (see Figure 1) have a concave spherical surface to form the cavity, and a convex ellipsoidal surface,

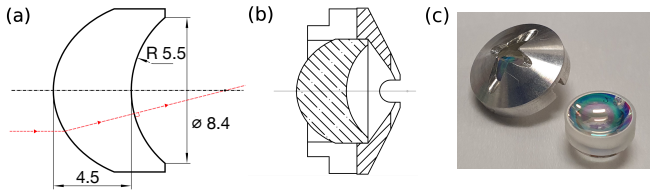

FIG. 1: Schematic of the cavity mirror: (a) with an example of ray propagation in red through the mirror (units in mm), (b) with the mirror mount, (c) corresponding pictures.

which provides a straightforward mode matching of a collimated input/output beam to the highly focused cavity mode[11]. The radius of curvature of the concave side is 5.5 mm, resulting in a cavity length $L_C = 2R - d$ in the NC regime, where R is the radius of curvature and d the (small) critical distance from the concentric point located at $L_C = 2R = 11$ mm. The mirrors have a reflectivity of $\mathscr{R} = 99.5\%$ at $\lambda = 780$ nm, corresponding to a cavity finesse of $F = 627$. The target noise limit factor $\xi = 0.15$ then corresponds to a cavity length fluctuation of $\delta L_{C,rms} \approx 0.9$ Å.

Cavity support structure

To accommodate the cavity mirrors, a structure that allows adjustment of three degrees of freedom of relative mirror positions is required. Moreover, it needs to fit within the constraints of the vacuum system. Additionally, the structure has to have a low susceptibility to external noise. To tackle these limiting factors, a tensegrity structure is chosen.

First, the cavity mirrors are fixed with epoxy to metal mirror mounts (see Figure 1 (b)), which protect the mirrors during handling, and shield them from the possible line-of-sight contamination from the atomic source. Gaps at the tip of the shield provide optical access for laser cooling beams to the center of the cavity where the atoms are trapped. The mirrors in their mounts are fixed to aluminum frames. These are separated by piezoelectric actuators (PI PICMA P-882.51) with a rectangular profile, forming the compression members of the tensegrity structure. Different orientations of these actuators with respect to the frames were evaluated.

To implement the tension members, two alternatives are tested. The first alternative used a 0.4 mm thick, laser-cut steel sheet, bent to a clip to hold the two mirror frames together. The clamp is designed such that only 3 points are in contact with the structure (see Figure 3 (a)). The second alternative used helical springs (MISUMI AUT3-20), with contact points defined by the hooks of the springs (see Figure 2 (c) and (d)).

One of the mirror frames is glued (MasterBond EP21TCHT-1) on a stainless steel plate to avoid applying pressure onto the structure when handling it during installation in the vacuum chamber, while the other frame can move freely in order not to constrain the relative tip-tilt movement of the mirrors.

The piezoelectric actuators have a maximal expansion of 15 µm for an operating voltage of 100 V, sufficient to compensate for misalignment after careful pre-alignment. Transverse misalignment can be corrected via different expansion rates of the three actuators, leading to a relative tip-tilt motion of the mirrors (see Figure 2 (a) and (b)). To allow for independent correction mechanisms for different degrees of freedom, the tip/tilt corrections T_{tip} and T_{tilt} as well as an overall cavity length change ΔL_C are combined to the respective actuator voltages $V_{A,B,C}$:

$$\begin{pmatrix} V_A \\ V_B \\ V_C \end{pmatrix} = G \begin{pmatrix} 1 & 1 & 1 \\ 1 & -1 & 1 \\ 1 & 1 & -1 \end{pmatrix} \begin{pmatrix} \Delta L_C \\ T_{tip} \\ T_{tilt} \end{pmatrix} \tag{2}$$

where G is a constant representing the transducer gain. This allows for both fast changes of the cavity length and a slower servo mechanism to maintain transverse cavity alignment[12].

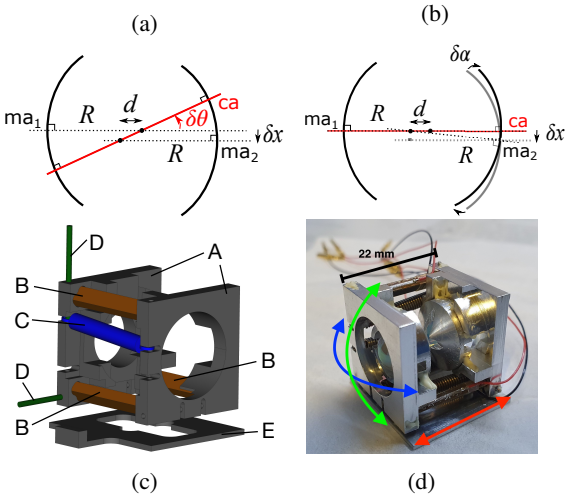

FIG. 2: (a): Rotation of cavity axis due to transverse misalignment. In a NC cavity of critical distance d, a small transverse misalignment δx of the second mirror rotates the cavity axis by an angle $\delta\theta$. (b): Equivalence of transverse and angular misalignment. A small transverse misalignment δx can be corrected by rotating the mirror by a small angle $\delta\alpha$. (c) CAD drawing. A: mirror frames. B: actuators. C: spring. D: metal rod. E: transportation plate. (d) Assembled NC cavity.

Different support structure configurations

The small expansion range of the piezoelectric actuators limits the correction range for transverse misalignment. As large transverse displacements can occur in the cavity structure during the assembly process (epoxy curing, baking of the vacuum chamber), the structure needs careful pre-alignment. A significant aspect of this pre-alignment is the static deformation of the compression structures due to the tension elements, and a consequent transverse misalignment. Thus, it is necessary to check and reduce the transverse misalignment resulting from the operation of the actuators.

To evaluate the transverse displacement in the different directions with regards to individual excitation of each actua-

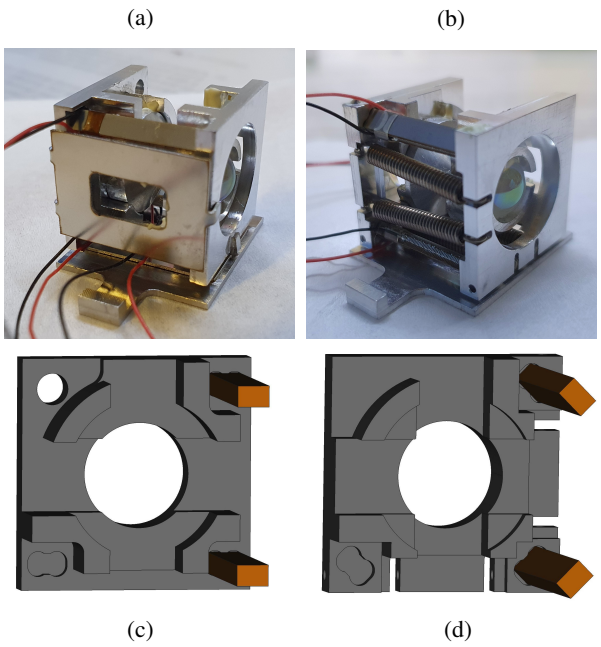

FIG. 3: (a) Structure using a 3 contact point clamp. (b) Structure using springs. (c) Actuator base parallel to the mirror frame. (d) Actuator base rotated by 45° from the mirror frame.

tor, one mirror frame is fixed in place with a clamp, and the displacement of the second mirror frame is measured with a microscope (with a $\times 10$ magnifying objective imaged onto a CCD camera (Point Grey CM3-U3-13S2M-CS)). The displacements of each structure configuration is listed in Table I. The helical springs show a much smaller transverse misalignment when added to the structure than the flat clip. We believe this is because the contact points and the static forces of the clips are not as well defined as the ones from the springs, with their spring constant tolerance of $\pm 10\,\%$.

Likely due to the actuator's rectangular cross section ($2\,\mathrm{mm} \times 3\,\mathrm{mm}$), an anisotropic bending behavior is observed, with greater flexural deformation along one axis. Rotating the the actuators with respect to the frame orientation (see Figure 3 (c) and (d)) significantly reduced the transverse displacement (see Table I).

TABLE I: Transverse displacement for several structure configurations.

Structure configuration	Maximum observed transverse displacement
Clamp (Figure 3 (a))	3.75 µm
Spring (Figure 3 (b))	1.25 µm
Parallel base (Figure 3 (c))	7 µm
45° base (Figure 3 (d))	3.75 µm

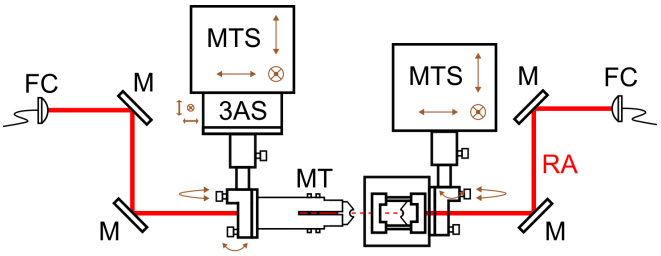

FIG. 4: Alignment setup of the NC cavity. RA: reference axis, FC: fibre coupler, M: mirror, MT: mechanical tweezer, MTS: manual translation stage, 3AS: three-axis actuator stage.

Cavity alignment

To assemble the near-concentric cavity, a reference axis is established by coupling light between two fiber couplers using four mirrors (see Figure 4). The cavity system, with the first mirror glued on using a low-outgassing epoxy (MasterBond EP21TCHT-1), is then fixed onto the right tip-tilt stage attached to a three-axis manual translation stage. The combination of the two stages allows the cavity mirror to be freely adjusted along the reference axis. The second mirror is held with a tweezer. The tweezer is also fixed onto the same type of tip-tilt stage as the first mirror, along with a three-axis piezoelectric translation stage with 100 µm moving range (Piezosystem Jena Tritor 101 CAP) for fine adjustment.

By maximising the coupling of the retro-reflected light from both cavity mirror convex surfaces back into the fibre couplers, each cavity mirror's axis is aligned along the reference axis (see Figure 4). The second mirror is then slowly translated towards the first mirror to form a cavity mode. The cavity mode and the transmission spectrum of the cavity are observed with a CCD camera and an amplified photodiode (Thorlabs PDA36A2). Any transverse misalignment is corrected using the three-axis piezoelectric translation stage.

The critical distance d can be estimated from the frequency spacing of the cavity transverse modes. The target critical distance is around $d \approx 7.8\,\mu\mathrm{m}$. This value is chosen as it is around half of the travel distance of the cavity's piezoelectric actuators, which will allow greater tip-tilt tuning as the cavity approaches concentricity.

Once the target critical distance is reached, mirrors are fixed to the frame with a small amount of epoxy, such that additional misalignment during the curing process is minimized. During the initial curing of the epoxy (2 hours), any misalignment is corrected using the three-axis piezoelectric translation stage. When the epoxy is fully cured after another 70 hours, the tweezer is released and removed.

CAVITY STABILITY

To characterise the susceptibility of the mounted cavity to external noise, the cavity resonance shift $\delta\omega_C$ is measured with respect to a laser which is loosely locked to the cavity with a Pound-Drever-Hall (PDH)[15] scheme through an inte-

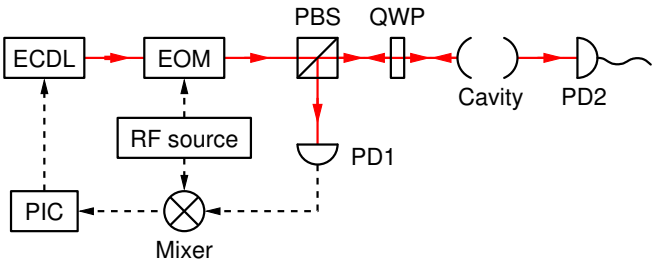

FIG. 5: Schematic of the experimental setup. ECDL: external cavity diode laser; EOM: electro-optical modulator; PIC: portional integral control; PBS: polarized beamsplitter; QWP: quater waveplate; PD: photodiode.

gral controller with small gain. With this method, fast cavity length changes at high frequencies can be measured, while ensuring that the error signal remains in the linear regime with respect to the length change δL_C, i.e., the mapping to frequency detuning stays injective.

The error signal from the PDH scheme is recorded with an oscilloscope and converted to a length change $\delta L_C(t)$. The noise spectral density of the recorded length change is shown in Figure 6. The total mechanical noise of the cavity system over the whole spectrum is $\delta L_{C,rms} = 0.36(9)$ Å, or a corresponding frequency uncertainty of $\delta\omega_C = 1.28(8)$ MHz.

The recorded error signal combines both laser noise and cavity noise. To separate the two contributions, the laser noise is characterised independently via modulation transfer spectroscopy[16] using a Rubidium vapour cell. The corresponding trace is shown in Figure 6 as well, with an integral total frequency uncertainty of $\delta\omega_{laser} = 0.11(3)$ MHz.

More than 70% of the total noise energy of the laser+cavity system is contained in a spectral window between 200 Hz and 2500 Hz, dominated by cavity contributions. This noise contribution could be caused by the susceptibility of transverse vibration modes of the springs to external noise, ultimately coupling to the cavity length.

To further enhance the system's stability, one can consider a stronger active stabilization scheme, in addition to the existing

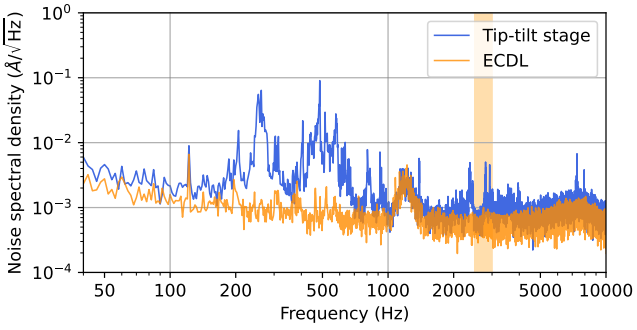

FIG. 6: Noise spectral density of the cavity length over an integration time of 0.5 s. Total noise is 0.36(9) Å. The shaded region highlights the first resonance of the cavity, centered at 2750 Hz (see Figure 7).

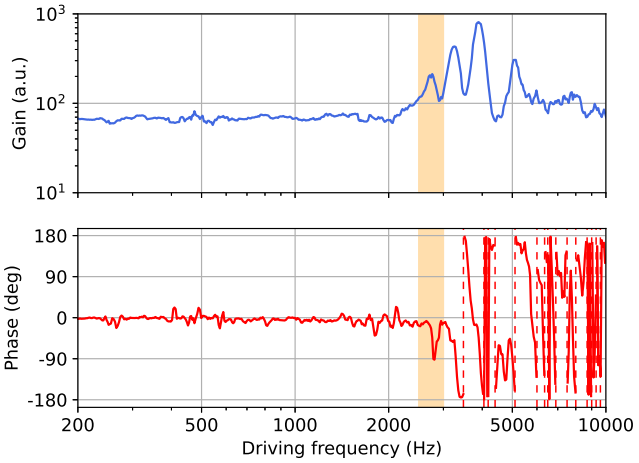

FIG. 7: Cavity response to the stimulus sent to the piezoelectric actuators. Shaded region highlights the first resonance of the cavity, centered at 2750 Hz.

loose I lock, for the cavity. This becomes feasible with access to a feedback signal for the cavity length, such as through the PDH scheme mentioned earlier. To implement this, we assess the cavity resonance response to an actuator length change stimulus at different frequencies.

A network analyzer (Agilent E5061b) generates this stimulus, which is added to the actuator's voltage, and picks up the error signal from PDH scheme in the same loose-lock configuration as above. The resulting Bode diagram of the system response is shown in Figure 7. A first resonance is observed around 2750 Hz, only contributing 1% of the total mechanical noise, with a fairly flat phase response below this resonance. Establishing a phase margin of 60° as the limit of the control for an active stabilisation implementation, an active length control of the NC cavity system up to a control bandwidth of ≈ 2500 Hz should be possible, removing the strong broad contribution up to 2000 Hz in the observed cavity noise spectrum. However, in our application, the passive effective cavity length uncertainty of $\delta L_{C,rms} = 0.36(9)$ Å is sufficient.

CONCLUSION

We implemented a passively stable compact structure for a near-concentric cavity, with an effective length uncertainty of 0.36(9) Å. This corresponds to a noise limit factor (see Equation 1) of $\xi \approx 0.05$. The passive stability permits an increase of the resonator's finesse while maintaining the cavity's stable relative to its linewidth, such that the system can operate effectively up to the last stable point of the concentric cavity. This increase in finesse will give access to even stronger atom–light interaction. Implementing an active cavity length stabilisation should suppress the susceptibility to external noise even further.

By relying purely on the current susceptibility to external noise of the cavity system, we can already enter the strong coupling regime with Rubidium atoms with a relatively low

finesse of 627. With the current cavity parameters, targeting the D_2 cycling transition of ^{87}Rb, the coupling strength can reach up to $g = 2\pi \times 17.3\,\mathrm{MHz}$, for a cavity decay rate of $\kappa = 2\pi \times 10.9\,\mathrm{MHz}$, leading to a maximum cooperativity of $C = g^2/2\kappa\gamma = 4.5$. This strong coupling will be used to explore atom–light interaction at the last near-concentric stable point.

In summary, we showed that the near-concentric cavity geometry can provide a viable alternative to near-planar cavity geometries for cavity-QED experiments, offering good optical access to the center of the cavity mode for atomic state preparation in quantum information processing schemes, and a large separation of mirror surfaces from the mode region with a strong field, reducing, e.g., the influence of charges on the mirror surfaces in ion trap configurations.

ACKNOWLEDGEMENTS

This work is supported by the National Research Foundation, Singapore, and A*STAR under project NRF2021-QEP2-01-P01/W21Qpd0101.

REFERENCES

[1] J. P. Covey, H. Weinfurter, and H. Bernien, "Quantum networks with neutral atom processing nodes," npj Quantum Information **9**, 90 (2023).

[2] L. J. Stephenson, D. P. Nadlinger, B. C. Nichol, S. An, P. Drmota, T. G. Ballance, K. Thirumalai, J. F. Goodwin, D. M. Lucas, and C. J. Ballance, "High-rate, high-fidelity entanglement of qubits across an elementary quantum network," Phys. Rev. Lett. **124**, 110501 (2020).

[3] Y.-S. Chin, M. Steiner, and C. Kurtsiefer, "Nonlinear photon-atom coupling with 4pi microscopy," Nature Communications **8**, 1200 (2017).

[4] C. Hamsen, K. N. Tolazzi, T. Wilk, and G. Rempe, "Strong coupling between photons of two light fields mediated by one atom," Nature Physics **14**, 885–889 (2018).

[5] A. Reiserer and G. Rempe, "Cavity-based quantum networks with single atoms and optical photons," Rev. Mod. Phys. **87**, 1379–1418 (2015).

[6] S. Haroche, "Nobel lecture: Controlling photons in a box and exploring the quantum to classical boundary," Rev. Mod. Phys. **85**, 1083–1102 (2013).

[7] J. Ye, D. W. Vernooy, and H. J. Kimble, "Trapping of single atoms in cavity qed," Phys. Rev. Lett. **83**, 4987–4990 (1999).

[8] C. J. Villas-Boas, K. N. Tolazzi, B. Wang, C. Ianzano, and G. Rempe, "Continuous generation of quantum light from a single ground-state atom in an optical cavity," Phys. Rev. Lett. **124**, 093603 (2020).

[9] M. Baghdad, P.-A. Bourdel, S. Schwartz, F. Ferri, J. Reichel, and R. Long, "Spectral engineering of cavity-protected polaritons in an atomic ensemble," Nature Physics **19**, 1104–1109 (2023).

[10] Z. Yan, J. Ho, Y.-H. Lu, S. J. Masson, A. Asenjo-Garcia, and D. M. Stamper-Kurn, "Super-radiant and sub-radiant cavity scattering by atom arrays," (2023), arXiv:2307.13321 [quant-ph].

[11] K. Durak, C. H. Nguyen, V. Leong, S. Straupe, and C. Kurtsiefer, "Diffraction-limited fabry-perot cavity in the near concentric regime," New Journal of Physics **16**, 103002 (2014).

[12] C. H. Nguyen, A. N. Utama, N. Lewty, and C. Kurtsiefer, "Operating a near-concentric cavity at the last stable resonance," Phys. Rev. A **98**, 063833 (2018).

[13] E. L. Raab, M. Prentiss, A. Cable, S. Chu, and D. E. Pritchard, "Trapping of neutral sodium atoms with radiation pressure," Phys. Rev. Lett. **59**, 2631–2634 (1987).

[14] R. Grimm, M. Weidemüller, and Y. B. Ovchinnikov, "Optical dipole traps for neutral atoms," (Academic Press, 2000) pp. 95–170.

[15] R. W. P. Drever, J. L. Hall, F. V. Kowalski, J. Hough, G. M. Ford, A. J. Munley, and H. Ward, "Laser phase and frequency stabilization using an optical resonator," Applied Physics B **31**, 97–105 (1983).

[16] D. J. McCarron, S. A. King, and S. L. Cornish, "Modulation transfer spectroscopy in atomic rubidium," Measurement Science and Technology **19**, 105601 (2008).